

---

# USING NEUROEVOLUTION FOR DESIGNING SOFT MEDICAL DEVICES

---

A PREPRINT

**Hugo Alcaraz-Herrera**

Unconventional Computing Laboratory,  
College of Arts, Technology and Environment,  
University of the West of England,  
Bristol, BS16 1QY, United Kingdom  
hugo.alcaraz@uwe.ac.uk

**Michail-Antisthenis Tsompanas**

Unconventional Computing Laboratory &  
School of Computing & Creative Technologies,  
College of Arts, Technology and Environment,  
University of the West of England,  
Bristol, BS16 1QY, United Kingdom  
antisthenis.tsompanas@uwe.ac.uk

**Andrew Adamatzky**

Unconventional Computing Laboratory,  
College of Arts, Technology and Environment,  
University of the West of England,  
Bristol, BS16 1QY, United Kingdom

**Igor Balaz**

Laboratory for Meteorology, Physics and Biophysics,  
Faculty of Agriculture,  
University of Novi Sad,  
Trg Dositeja Obradovica 8, 21000, Novi Sad, Serbia

August 20, 2024

## ABSTRACT

Soft robots can exhibit better performance in specific tasks compared to conventional robots, particularly in healthcare-related tasks. However, the field of soft robotics is still young, and designing them often involves mimicking natural organisms or relying heavily on human experts' creativity. A formal automated design process is required. We propose the use of neuroevolution-based algorithms to automatically design initial sketches of soft actuators that can enable the movement of future medical devices, such as drug-delivering catheters. The actuator morphologies discovered by algorithms like Age-Fitness Pareto Optimization, NeuroEvolution of Augmenting Topologies (NEAT), and Hypercube-based NEAT (HyperNEAT) were compared based on the maximum displacement reached and their robustness against various control methods. Analyzing the results granted the insight that neuroevolution-based algorithms produce better-performing and more robust actuators under different control methods. Moreover, the best-performing morphologies were discovered by the NEAT algorithm. As a future work aspect, we propose using the morphologies discovered here as test beds to optimize specialized controllers, enabling more effective functionality towards the desired deflections of the suggested soft catheters.

**Keywords** Neuroevolution · NEAT · HyperNEAT · AFPO · Catheter

## 1 Introduction

The concept of *soft robots* can be traced back to Isaac Asimov's books published in the 1940s-1950s. However, the first scientific and engineering papers related to soft grippers [20] and soft architecture machines [42] started in the late 1970s. The domain has started to flourish in late 1980s with further publications on soft fingers [3, 9, 10], electrostatic actuators [16], and fluid based grippers [25]. Unlike traditional and rigid robots, these robots are built utilising flexible and ductile materials [32, 50]. Soft robots have the potential to exhibit better performance in specific tasks that are related to search and rescue [39, 41, 62, 64], space exploration [38, 5, 43, 40], and healthcare [46, 33, 22] due to their mechanisms and morphology, which are inspired by the movement and behaviour of living organisms.

Publications on soft robotic catheters, and relevant surgical devices, started to emerge from late 1980s [29] and by 2020 there was a range of catheters developed for cardio-vascular surgery [45, 49, 44], urinary system [30, 8, 65], endovascular treatment [18], in situ bioprinting [67], endoscopy [31], drug delivery [23]. Plantoid robots proposed by Mazzolai and colleagues [35, 37, 15, 36, 34, 51] can be considered relevant to the research on robotic catheters. These robots are soft-bodied mechanical devices capable of physically growing at the tip (thanks to embedded 3D printing techniques), similar to a plant root, and can change the direction of their growth due to incorporated environmental condition sensors.

Although soft robotics is a promising research area with extensive applicability, it entails considerable challenges. One of the most intricate challenges is finding a proper design: finding the most suitable robot design requires substantial time and material resources because it implies numerous iterations of testing the design in real life [53]. Unfortunately, for soft robots, design and other aspects are more complex, since they use flexible materials whose mechanical properties are non-linear and complex to characterise [19]. For instance, *biohybrid machines*, a particular type of soft robots, are built employing biological components, such as cells or tissues, which are inherently difficult to control with conventional methods. This brings another set of challenges, since several parameters need to be considered during the design of these soft robots.

One promising strategy to counteract the intrinsic challenges of soft robots is the use of NeuroEvolution (NE). NE consists of evolving the topology and weights of artificial neural networks (ANNs) through a genetic algorithm (GA). One of the most effective and well-known approaches is NeuroEvolution of Augmenting Topologies (NEAT) [57], which has demonstrated an adequate performance regarding morphology generation [7]. Moreover, NEAT was extended under the rationale that natural structures are composed of patterns and shape repetition. This extension is called Hypercube-based NeuroEvolution of Augmenting Topologies (HyperNEAT) [56]. This new approach evolves a particular type of networks, i.e., Compositional Pattern-Producing Networks (CPPNs), which use, among others, periodic functions, such as sine and cosine, to generate symmetry and patterns that help to evolve topologies [55].

The primary objective of this research is to validate the suitability of NEAT and HyperNEAT as tools to design soft robot morphologies. Particularly an example is studied here of designing soft actuators of catheters for targeted drug delivery to areas of the human body that are difficult to reach. We chose the catheter scenario as an exemplary case study for automated morphology generation due to the simplicity and focus of its design. Catheters have limited degrees of freedom, so, the most critical factor in their morphology is bending. This streamlined focus on bending allows automated systems to concentrate on optimising flexibility, ensuring that generated models are both functional and adaptable to various medical scenarios.

Furthermore, the presented research can be considered the continuation of the study presented in [4], where, in terms of designing soft robots for locomotion-oriented tasks, the suitability of NEAT and HyperNEAT was tested. The validation methodology implemented in this research compares the performance of NEAT and HyperNEAT against Age-Fitness Pareto Optimisation (AFPO), an evolutionary algorithm designed to avoid premature convergence [21]. Three metrics are used to assess the performance of the algorithms: (i) the general performance in terms of the displacement observed in one end of the actuators during a specific time-frame; (ii) the robustness of the designs of actuators produced; and (iii) the total volume of actuators.

The rest of the paper is organised as follows. Section 2 describes background research focusing on soft-robot-related tasks utilising NEAT and HyperNEAT algorithms. Section 3 introduces in detail the mechanisms of the three algorithms utilised for experimentation in this research. Section 4 describes the experiments performed in the task of designing soft actuators for catheters. Finally, Section 5 concludes this work by presenting insights that emerged from the research and outlines future work.

## 2 Background

NEAT has been implemented in numerous studies focusing on soft-robot-oriented tasks. An example of these studies presents a three-link planar arm model driven by nine muscles, whose purpose is to simulate the human arm [63]. A neurocontroller trained by NEAT controls the muscular-skeleton arm. The training sets applied to NEAT are built considering the forward kinematics, geometry relationships, and muscle mechanic equations. NEAT is compared against a fixed-topology ANN. Results indicate that the neurocontroller trained by NEAT outperforms the traditional ANN in critical aspects such as moving the arm to a specific position and converging the distance between the endpoint and the target point with a minimum distance error.

NEAT has not only been studied for controlling bioinspired mechanisms. It also has been utilised as a design engine for soft robots. For instance, in [11], NEAT, alongside CPPNs, is utilised to design soft robots capable of reaching or squeezing through a small aperture. The experiments consisted of simulations where each soft robot is placed within a

cage whose dimensions are  $15 \times 15 \times 11$ , leaving a gap of 1 voxel (arbitrary volume in the physics simulator) in the  $x$  and  $y$  axes between the edge of the cage and the maximum size of the soft robot:  $11 \times 11 \times 11$ . The cage is rigid, immobile and indestructible. Each side has an opening, approximately a circle of diameter 10. Although this research is primarily considered as a proof-of-concept, it is demonstrated that more compliant and deformable soft robots are more capable of reaching or squeezing through small apertures, such as tunnels, than soft robots that are less flexible.

Following the same path of being utilized as morphology generator, in [6], NEAT (and CPPNs) is used to produce three-dimensional physical structures capable of conserving momentum to achieve maximum displacement due to gravity. Structures are composed of spherical cells which fuse to make rigid bodies. The growth process commences with a single cell called *root* and is located at the origin of the structure. A cloud of  $n$  points is set around the cell with the  $n$  points distributed on the root's surface. Once the cloud is over the cell, every point is used to query a CPPN whose output represents the concentration of matter at that point. A matter threshold determines where to allocate a cell: the more the output value exceeds the matter threshold, the denser the cell allocated at that point will be. Results suggest that the proposed method can produce artefacts that suitably capture the non-obvious relationship between function and physical structure.

Another study where NEAT helps to design morphologies of soft robots capable of navigating across environments with different levels of viscosity is described in [24]. The approach consists of evolving ANNs that observe the virtual environment and respond to it by controlling the muscle force of the soft robot. The performance of morphologies is tested in three different environments: (i) low-viscosity drag; (ii) intermediate-viscosity drag; and (iii) high-viscosity drag. Results indicate that the properties of the environment have a strong influence on soft robot design. For instance, it is possible to observe that the evolutionary pressure flats the parts with big surfaces of the morphologies, which exploits the viscosity drag [24].

NEAT has not only been used for soft robots focused on one task. In [26], this method is utilised to build morphologies of soft robots capable of performing more than one specific task. The study argues that by combining the genotype of soft robots focused on single-functional tasks is feasible to generate multi-functional robots. The experiments involved in this study consisted of simulating voxel-based creatures performing tasks in terrestrial and aquatic environments. Results suggest that the proposed method: (i) enables the efficient exploration of the morphology search space; (ii) can find morphologies that satisfy two tasks simultaneously faster than existing methods.

On the other hand, HyperNEAT has been primarily utilised in tasks targeting the control of robot morphologies. An example of these studies presents a method where morphologies are the input, and the output is neural network controllers capable of working on these different morphologies [48]. Each neural controller is tested in three different quadruped morphologies whose lengths are 0.25, 0.30, and 0.37 meters. The neural controllers generated by HyperNEAT are compared against static controllers. Results indicate that HyperNEAT can identify the relationship between morphology and controller architectures during evolution, which leads to a suitable performance.

In the same direction of controller design, in [12], a study that refers to legged robots, particularly four-legged, is presented. The rectangular torso of the robot morphology is 0.15 wide, 0.3 long, and 0.5 tall (in arbitrary ODE physics simulator units). Each leg has three cylinders (radius 0.02, length 0.075) and three hinge joints. HyperNEAT is compared against *Fixed-Topology* NEAT (FT-NEAT), also known as Perceptron NEAT. Results indicate that HyperNEAT outperforms FT-NEAT since its morphologies: (i) vastly outperform those generated by FT-NEAT in every generation and (ii) exhibit better coordination than those created by FT-NEAT. Another relevant insight of this research is that generative encodings can outperform direct encodings on regular problems.

Another study, described in [66], focuses on creating gaits for quadruped robots. HyperNEAT is compared against six parameterised learning strategies: (a) uniform random hill climbing; (b) Gaussian random hill climbing; (c) policy gradient reinforcement learning; (d) Nelder-Mead simplex; (e) a random baseline; and (f) a new method that builds a model of the fitness landscape with linear regression. Nine servos actuate the robot used for experimentation, each commanded to a position in the  $[0, 1023]$  range, corresponding to a physical range of  $[-120^\circ, +120^\circ]$ . Two on-board batteries power the servos. Results advocate the superiority of HyperNEAT over all parameterised learning strategies since the gaits it generates exhibit significantly better performance.

Not only one neurocontroller can be evolved through HyperNEAT. In [14], it is stated that it is possible to evolve neurocontrollers encoded by a single genome representing a team of predator agents that work together to capture prey. In the experiments conducted, agents are not aware of their teammates, and due to prey avoidance from nearby predators, it is feasible for one predator to undermine another's pursuit by knocking its prey off its path. Consequently, predators are forced to learn coherent roles that complement the roles of their allies. Results indicate that encoding a team of agents as a unified genome brings benefits such as: (i) critical skills do not need to be rediscovered for separate agents; (ii) due to CPPNs representing multiagent policies, they are assigned to separate agents as a function of their relative geometry and simultaneously exploiting the internal geometries of agents.

HyperNEAT has been scarcely used to design morphologies of soft robots. For instance, in [58], HyperNEAT is employed to evolve controllers and morphologies simultaneously. Robots are evaluated considering their capabilities to adapt in four different scenarios: (i) moving in a flat terrain in a limited time; (ii) moving in a highly uneven terrain; (iii) climbing through a narrow stepwise channel; and (iv) throwing a solid box. Results suggest that the method generates robots that show a suitable performance in all the aforementioned tasks.

More recently, another study tests the suitability of HyperNEAT (and NEAT) as a design engine for soft robot morphologies, which is described in [4]. The experiments focused on locomotion tasks, particularly reaching the maximum displacement possible in 10 seconds. Morphologies generated by AFPO are utilised as a baseline. Results indicate that neuroevolution-based approaches can outperform AFPO, and HyperNEAT can perform more suitably than NEAT, despite the absence of geometrical aspects of the problem domain in the design of the substrate. This confirms what is argued in [13]: HyperNEAT can obtain suitable results, even if there is no defined geometrical representation of the problem.

Thus, based on the previously analysed research findings, it is feasible to consider NEAT and HyperNEAT as the core strategy to design adequate morphologies for soft actuators for catheters.

### 3 Algorithms

Three algorithms were utilised in this research. Namely, Age-Fitness Pareto Optimisation (AFPO), NeuroEvolution of Augmenting Topologies (NEAT), and Hypercube-based NeuroEvolution of Augmented Topologies (HyperNEAT), which will be described in Section 3.1, Section 3.2, and Section 3.3 respectively.

#### 3.1 AFPO

This approach was conceived as an alternative method to avoid premature convergence in evolutionary algorithms [52], an issue exhibited by other evolutionary approaches. One of the fundamental aspects of AFPO is *age*, which, under this scope, can be understood as how long genotypic material has existed in the population [21]. Based on this, the age of a solution (i.e., an individual) is measured in generations.

The algorithm commences initialising the individuals composing the population at random, with age of all individuals set to one. If an individual survives to the next generation, its age is incremented by one. When genetic operators (i.e., crossover and mutation) take place, the age is inherited as the maximum age of the parents.

Since AFPO employs a single population, it tracks each individual's fitness similarly to a standard evolutionary algorithm, including the genotypic age. The multi-objective optimisation procedure aims to determine the non-dominated Pareto front of the problem domain, where the objective is maximising fitness with minimum age. One way of visualising the mechanism of AFPO is the population (i.e., individuals) evolving in a two-dimensional plane of age and fitness. Figure 1 illustrates this dynamic.

#### 3.2 NEAT

This algorithm was designed to counteract on three main issues that previous NE algorithms exhibit: (i) a solution representation capable of allowing arbitrary topologies to recombine; (ii) avoiding the premature disappearance of topological novelties discovered throughout the evolutionary process; and (iii) avoiding complex topologies without using a fitness function focused on punishing topological complexity [57].

The first issue was tackled using *gene tracking by historical markings*. This is achieved with a list of connection genes which represent a connection between two nodes containing: (a) the “origin” node and the “destination” node, (b) the weight of the connection, and (c) a Boolean state of the connection (enabled or disabled). Moreover, each gene has one *global innovation number*, a unique numerical ID and the core of the crossover operator.

Two genes having the same global innovation number (also known as “historical origin”) represent the same structure; therefore, the genes of both genomes that have the same innovation number are aligned. The genes that do not match are inherited from the fittest genome or chosen at random. When a new gene is generated by mutation, the global innovation number increases and is associated with the new gene. Innovation numbers are generally the chronology of every gene during the evolutionary process. Figure 2 presents an example of a genotype (i.e., a neural network) and its associated phenotype.

The second issue, was addressed by *speciation to protect innovation*, which generates species within the population aiming at the interaction of individuals that belong to the same species. NEAT creates species utilising topological similarities that are identified by the use of historical markers. The canonical way to measure compatibility of two

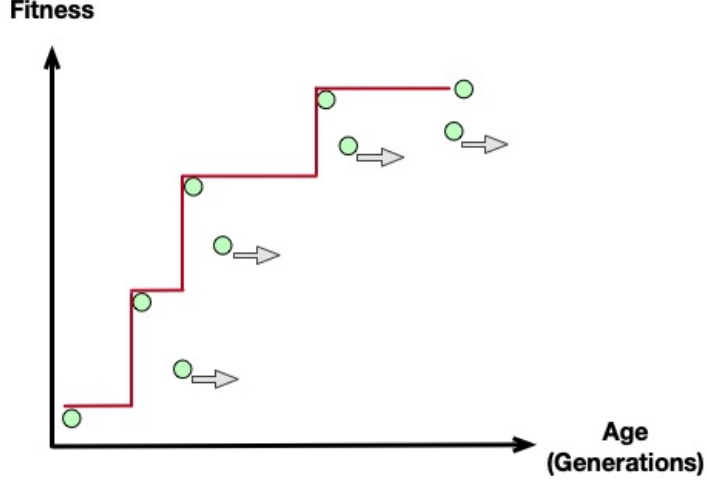


Figure 1: An example of a population moving in a two-dimensional Pareto space where the vertical axis is fitness and the horizontal axis is age. Figure adapted from [52].

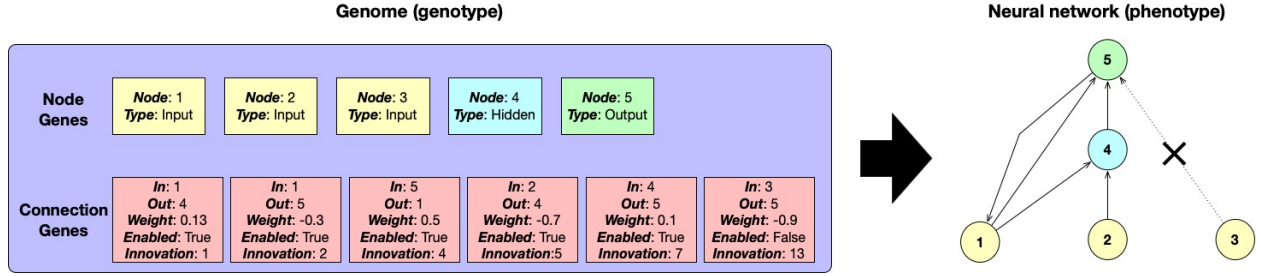


Figure 2: Example of a genotype and its phenotype under NEAT. Figure adapted from [54].

genomes (i.e., individuals) is by the number of excess and disjoint genes. Thus, the less disjoint genes are, the more compatible the two individuals are. The compatibility distance ( $\delta$ ) between two genomes is as follows [54]:

$$\delta = \frac{c_1 E}{N} + \frac{c_2 D}{N} + c_3 \times \bar{W} \quad (1)$$

where  $E$  is the number of excess genes,  $D$  represents the disjoint genes,  $\bar{W}$  is the mean weight differences of matching genes,  $c_1$ ,  $c_2$ ,  $c_3$  are utilised to determine the relevance of  $E$ ,  $D$ , and  $\bar{W}$ , respectively. Regarding  $N$ , it represents the number of genes in the individual with the largest number of genes; it is used to normalise the genome size during the evolutionary process. The distance  $\delta$  determines in which species an individual is allocated utilising a compatibility threshold  $\delta_t$ . Individuals are allocated into the first species (taken at random) where their distance  $\delta$  is  $< \delta_t$ , assuring that individuals do not belong to more than one species.

NEAT evaluates individuals utilising *explicit fitness sharing*. Under this schema, individuals within the same species share the fitness, which implies a limitation for species to expand over the population [17]. Since this mechanism adjusts the fitness of individuals by dividing an original fitness by individuals in each species, the species grow or shrink if their average adjusted fitness is either over or under the population average.

The third issue was alleviated by *minimising network structures*, which is feasible due to the mechanism of speciation to protect innovation. Since NEAT can initialise individuals whose input neurons are fully connected to the output neurons (i.e., no hidden nodes are involved), new structures are incrementally generated when structures are mutated during the evolutionary process. The structures that exhibit a suitable performance can survive. The effect induced by this approach narrows down the search towards a minimal number of weight dimensions, which implies: (a) a reduction of runtime to find solutions [59] and (b) avoiding the generation and evaluation of complex structures during the evolutionary process.

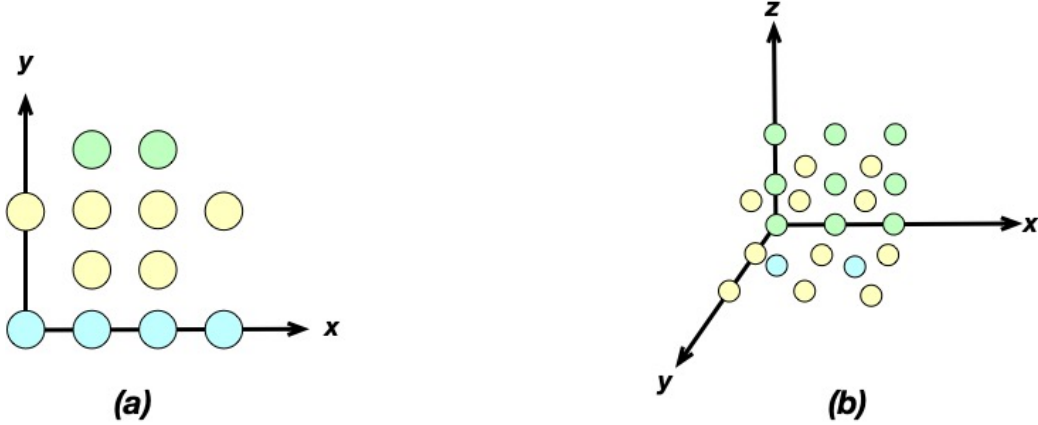


Figure 3: Two typical configurations of substrates utilised in HyperNEAT: (a) two-dimensional, and (b) three-dimensional.

### 3.3 HyperNEAT

This approach is an extension of NEAT [56], which utilises the evolutionary engine of the aforementioned algorithm to evolve a particular class of neural networks known as CPPNs [55]. CPPNs are used due to their ability to generate patterns, such as repetition and symmetry. There exist two key differences between NEAT and HyperNEAT:

1. *Activation functions.* Typically, NEAT generates ANNs containing hidden nodes exclusively using the sigmoid function. HyperNEAT, nevertheless, allows the use of other activation functions, such as Gaussian, trigonometric, and periodic, in the nodes composing CPPNs. In this way, CPPNs can evolve, exploring a significantly more expansive search space of network topologies.
2. *Substrate.* HyperNEAT is capable of embodying the geometry of the domain problem due to the nature of CPPNs; therefore, the topology of ANNs is computed, taking into account their geometry. Thus, the geometric layout where HyperNEAT operates is called a *substrate*, which can be configured in diverse manners. One of the most popular configurations consists of a set of nodes allocated in a two-dimensional plane; it is known as *grid*. Another widely used configuration is the *three-dimensional grid*, which contains a set of nodes allocated in a three-dimensional space. Figure 3-a depicts an example of a grid, whereas Fig. 3-b presents an example of a three-dimensional grid.

Under HyperNEAT, topologies of ANNs embodied in the substrate are generated by CPPNs employing the position of the neurons. Consequently, when a two-dimensional substrate is used, the weight between the neuron  $m$  and the neuron  $h$  is calculated using their position in the substrate:

$$CPPN(x_m, y_m, x_h, y_h) = weight_{mh} \quad (2)$$

Regarding the bias of neurons, they are computed, providing the coordinates of the neuron in the “origin” position, whereas the “destination” coordinates are set to zero. Thus, the bias of neuron  $m$  is obtained by:

$$CPPN(x_m, y_m, 0, 0) = bias_m \quad (3)$$

Furthermore, if a three-dimensional grid is being utilised, the weight between the neuron  $h$  and the neuron  $m$  is computed as follows:

$$CPPN(x_h, y_h, z_h, x_m, y_m, z_m) = weight_{hm} \quad (4)$$

The bias of neurons is calculated analogously to the manner described in Equation 3. Therefore, the bias of neuron  $h$  is calculated by:

$$CPPN(x_h, y_h, z_h, 0, 0, 0) = bias_h \quad (5)$$

Table 1: Parameters utilised to evolve CPPNs under NEAT and HyperNEAT for the actuator generator domain.

Parameter	Value
compatibility threshold	3
compatibility disjoint coefficient	1.0
compatibility weight coefficient	0.5
maximum stagnation	25
survival threshold	0.6
activation function mutate rate	0.4
adding/deleting connection rate	0.3/0.2
activating/deactivating connection rate	0.5
adding/deleting node rate	0.3/0.2

In general, the mechanism of HyperNEAT starts by defining the substrate. The next step consists of generating the initial population of CPPNs. Then, for each CPPN, the connections (i.e., weights) and bias of the substrate are calculated using Eqs. 2 and 3 for a two-dimensional grid, and Eqs. 4 and 5 for a three-dimensional grid. Once the substrate is built, its performance (and hence the performance of the CPPN) is evaluated, and a fitness score is assigned to the CPPN. After the evaluation stage, NEAT is applied to evolve the population of CPPNs. It is important to emphasise that the outputs of CPPNs are usually in the  $[-1.0, 1.0]$  range, which, in case it is necessary, implies a normalisation or mapping procedure.

Summarising, HyperNEAT aims to evolve the topology (i.e., the connectivity) and weights of ANNs that are represented by a substrate with a specific geometry through CPPNs.

## 4 Actuators generator

In this research, three metrics are used to determine the suitability to generate soft actuator morphologies of NEAT and HyperNEAT: (i) the general performance in terms of the displacement of the actuator in the  $yz$  plane during a simulated time period; (ii) the robustness of the fittest actuators found; and (iii) the number of voxels composing the actuator. Furthermore, AFPO (see Section 3.1) is utilised as a baseline actuator generator in these experiments, and the implementation employed is available on GitHub [2] and is fully described in [28].

### 4.1 Experimental setup

The population is composed of 100 individuals (i.e., CPPNs) for the three approaches. Each evolutionary run lasted 3000 generations. The set of activation functions utilised for experimentation is the same as used in [28], and is composed of: *sigmoid*, *sine*, *negative sine*, *square*, *negative square*, *square root of absolute*, *negative square root of absolute*, *absolute*, and *negative absolute*. Activation functions are randomly chosen during CPPN initialisation and mutations. In order to perform a fair comparison for all approaches, the implemented initialisation procedure of the population is described in [28]. Moreover, for NEAT and HyperNEAT, the parameters employed for the evolutionary process of CPPNs are shown in Table 1. For each approach, 20 independent experimental runs were performed, by changing only the initial random populations.

The fitness function consists of a physics engine called *Voxelyze* (also available in [2]), which simulates the physical response of morphologies under determined conditions. Morphologies are defined within Voxelyze by stacking voxels (the minimum building block in Voxelyze) of different materials together. Here two types of voxels were considered for simplicity of the designing landscape, namely one active voxel and one passive voxel. The original version of Voxelyze was modified (changes in the source code available in [1]) to trace the position of the catheter actuator in the  $x, y, z$  axes during a time  $t$ . Furthermore, one end of actuators is fixed in such a way that they only move vertically (i.e., one degree of freedom) in the  $yz$  plane. In addition, actuators have a passive enclosure to follow the findings of previous simulation works [60] and constraints of laboratory experiments, i.e. the bioreactor that a muscle actuator need to provide nutrients. The output of Voxelyze contains three values that describe the position of the actuator free tip (with respect to  $x, y, z$  dimensions) for the initial position and the final one (after the predefined simulation time), and the number of voxels that compose the actuator.

Regarding the dimensions of actuators, in terms of voxels, there are 20 units in the  $x$  axis and 8 units in the  $y$  and  $z$  axes. Thus, the axes range of the three-dimensional layout where morphologies are designed are as follows: for  $x$  axis,  $[0, 20]$ . For  $y$  and  $z$  axes,  $[0, 8]$ .

Since simulations require a significant amount of computation time, it is essential to try to reduce it. Thus, the implementation related to AFPO was written under the multiprocessing paradigm [28]. The implementation used for NEAT and HyperNEAT was designed under a client-server architecture to take advantage of its distributed computing capacities. The full description of the client-server implementation utilised in this research can be found in [4]. Finally, the hardware utilised for experimentation is: *Processor*: ARM (virtualised), nine cores (18 threads), 3.20GHz, *RAM Memory*: 16GB, LPDDR5.

#### 4.1.1 NEAT configuration

Due to actuators being designed in a discrete three-dimensional layout, it is necessary to provide for each point across the layout: (i) the presence or not of a material voxel, and (ii) the material type the voxel is made. Thus, under NEAT, CPPNs are queried as follows:

$$CPPN(x_i, y_i, z_i) = v_i, m_i \quad (6)$$

where the tuple  $(x_i, y_i, z_i)$  represents the coordinates of the  $i$ -th point in the three-dimensional layout,  $v_i$ , refers to the presence of a voxel in the  $i$ -th point of the layout, and it is processed as the presence or absence of a voxel by the following equation:

$$Presence(x_i, y_i, z_i) \begin{cases} \text{yes,} & |v_i| \geq 0.5 \\ \text{no,} & \text{otherwise} \end{cases} \quad (7)$$

Furthermore,  $m_i$  represents the type of material of the voxel in the  $i$ -th point of the layout. In the scope of this research, two types of materials are considered: (i) *passive*, encoded as 1, and (ii) *contractile*, encoded as 3. Equation 8 presents the mechanism to map  $m_i$  as an encoded material ID.

$$Material\ code(x_i, y_i, z_i) \begin{cases} 1, & |m_i| < 0.5 \\ 3, & \text{otherwise} \end{cases} \quad (8)$$

#### 4.1.2 HyperNEAT configuration

The first element of HyperNEAT to determine is the substrate. Thus, based on the discrete three-dimensional layout used to design actuators, the substrate has three neuron inputs. Furthermore, since the data required to determine the presence of a voxel in the  $i$ -th point and the material of that voxel, the number of output neurons is two. Equation 9 presents how substrates are queried.

$$substrate(x_i, y_i, z_i) = v_i, m_i \quad (9)$$

where the tuple  $(x_i, y_i, z_i)$  is the coordinates of the  $i$ -th point in the three-dimensional layout. The  $v_i$  variable is associated with the presence or absence of a voxel in the  $i$ -th point of the layout and is mapped using Eq. 7, and  $m_i$  is related to the type of the voxel material in the point  $i$  of the layout and is processed by Eq. 8. Figure 4 depicts the design of the two-dimensional substrate used for experimentation. The neuron allocation used for the substrate was found by conducting a series of experiments varying the number of neurons per hidden layer and the number of hidden layers in the  $[1, 5]$  range. Furthermore, the activation function implemented in the substrate is *SELU* due to its fast convergence and self-normalising properties [27].

Once the substrate is defined, the following step defines how CPPNs are queried. Since the substrate was defined in a two-dimensional space, CPPNs are queried utilising Eq. 2 for calculating the weights among neurons, and Eq. 3 to compute the bias of the neurons allocated in the substrate. It is essential to point out that based on the definition of HyperNEAT [61], determining whether a connection is calculated is by a threshold. Thus, if  $|weight_{mh}| > 0.2$ , it is normalised in the  $[-3.0, 3.0]$  range. Otherwise, there is no connection between the neuron  $m$  and the neuron  $h$ .

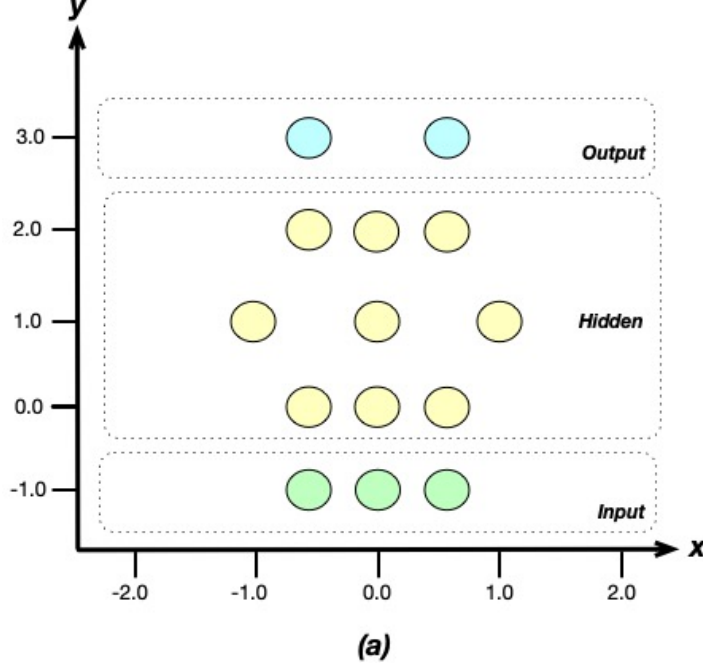


Figure 4: Substrate employed under HyperNEAT for actuator generator.

## 4.2 Analysis of the performance

In order to validate the suitability of catheter actuators generated by AFPO, NEAT and HyperNEAT, three experiments are conducted: (i) analysing the general performance in terms of finding the actuator with the maximum displacement possible (i.e., the fittest) in the  $yz$  plane; (ii) testing the robustness of the fittest actuators found; and (iii) identifying the fittest actuators with the minimum volume (i.e., the minimum number of voxels) possible. It is essential to highlight that during all experimentation stages, the displacement was measured in terms of the length of voxels.

### 4.2.1 Finding the fittest actuator

One vital feature of actuators is the displacement in the  $yz$  plane, since they have one end fixed. This displacement can be understood as an indicator of the bending capacity exhibited by actuators: the more displacement the actuator reaches, the more bendable the catheter is. This capability is crucial because catheters can deliver drugs from diverse angles. Hence, the more bendable the actuator is, the higher the agility of the drug delivering catheter.

In this experiment, the evaluation of actuators is as follows: for each independent experimental run, 25 different controller phase offsets are generated at random and do not change over time. For each morphology of the population, the 25 controller phase offsets previously generated are used to simulate the displacement of the actuator. In other words, each morphology is simulated 25 times with different controller phase offsets. This procedure occurs each generation until the experimental run is complete. Thus, the aptitude ( $apt$ ) of the actuator  $a$  is calculated as follows:

$$apt_a = \frac{\sum_{i=1}^{25} displacement_i}{25} \quad (10)$$

It is important to emphasise that this experiment does not consider the number of voxels as a penalty for the aptitude value.

Figure 5 shows the mean performance in finding the fittest individual (i.e., the fittest actuator) with 95% confidence intervals depicted by the shaded regions across 20 experimental runs under AFPO, NEAT and HyperNEAT. In general, AFPO exhibits a significantly better performance than both neuroevolution-based approaches. Furthermore, NEAT performs better than HyperNEAT. All the data gathered were tested and are not normally distributed (Shapiro-Wilk test;  $p < 0.01$ ). Using the Kruskal-Wallis test, it is feasible to confirm that significant differences exist among the

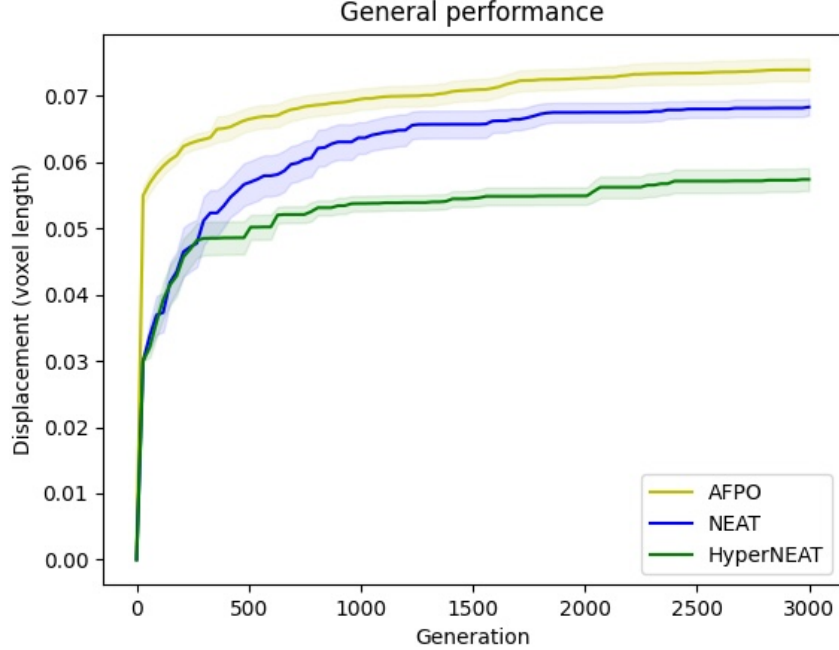


Figure 5: Mean performance of AFPO, NEAT, and HyperNEAT showing  $\pm 95\%$  confidence interval (shaded region).

performance of the three approaches ( $p < 0.01$ ). Therefore, a ranking in terms of performance can be performed: AFPO > NEAT > HyperNEAT (Dunn's test:  $p < 0.01$ ).

These results suggest that under 25 different controller phase offsets, AFPO can find the fittest actuators morphologies than those found by NEAT and HyperNEAT. Moreover, HyperNEAT's unexpected performance may be influenced by the absence of domain geometric elements that can be embodied in the substrate design.

#### 4.2.2 Exploring the robustness of the fittest actuator

A catheter could be suitable to deliver drugs in numerous angles under a specific scenario (i.e., a specific controller phase offset of each active voxel composing the actuator). However, it might not exhibit similarly high performance if the scenario changes. This experiment focuses on testing the robustness (i.e., how suitable the performance is regardless of the external conditions) of the three fittest actuators found across the 20 experimental runs conducted using AFPO, NEAT and HyperNEAT.

Each top actuator generated by all approaches is tested utilising 1000 different controller phase offsets of each active voxel. In other words, the controller phase offset scenarios were randomly generated and used by all the morphologies implied in this experiment (i.e., the three fittest actuator morphologies generated by each approach). Thus, the robustness of the actuator  $a$  can be measured through a modified version of Eq. 10, which is defined as follows:

$$apt_a = \frac{\sum_{i=1}^{1000} displacement_i}{1000} \quad (11)$$

Figure 6 presents violin plots comparing the performance (i.e., the displacement observed in the  $yz$  plane of the free end of the morphology) of the three fittest actuators found by AFPO, NEAT and HyperNEAT. Each violin plot exhibits the maximum, minimum, median and kernel density estimation of the frequency distribution of values under 1000 different offset controller scenarios.

When AFPO is applied (see Fig. 6-a), all morphologies exhibit significant differences, which is determined by testing all the data collected, and they are not normally distributed (Shapiro-Wilk test;  $p < 0.01$ ). Ten by the Kruskal-Wallis test, it is possible to confirm significant differences among the displacement observed in the three actuators ( $p < 0.01$ ). Thus, a performance ranking can be performed: Morphology 12 > Morphology 19 > Morphology 7 (Dunn's test:  $p < 0.01$ ).

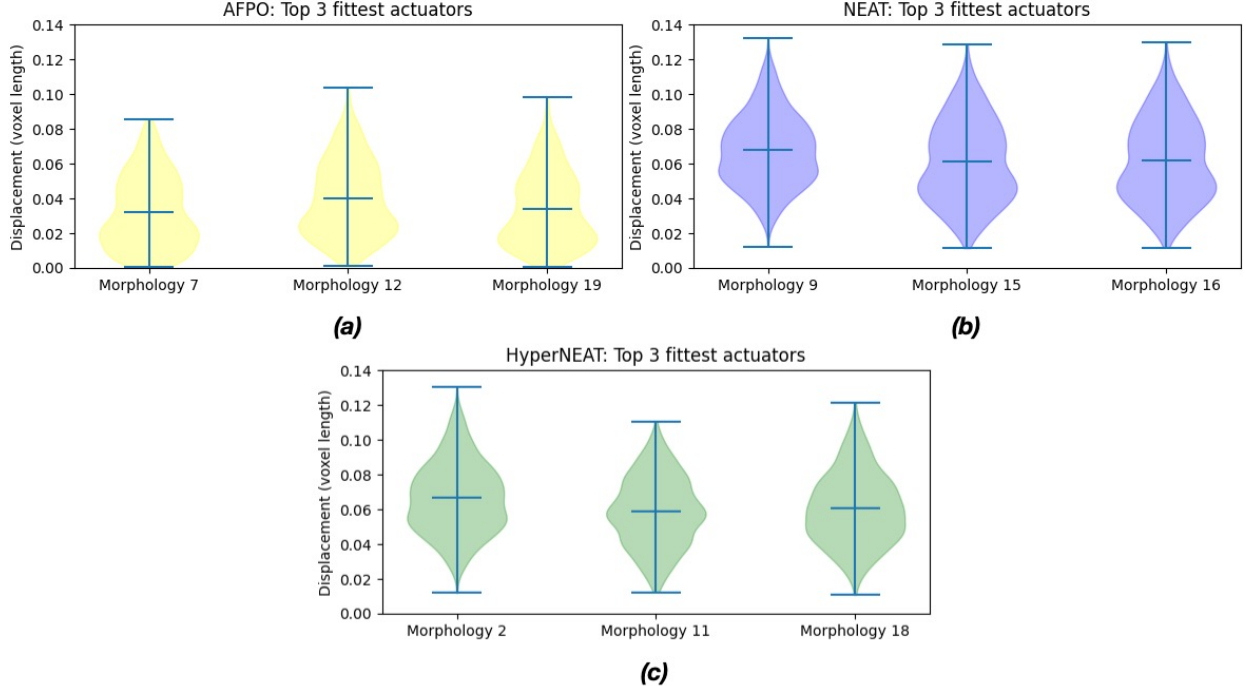


Figure 6: Displacement observed in the  $yz$  plane under 1000 different controller phase offset controllers of the top three fittest actuators found in 20 different experimental runs under: (a) AFPO; (b) NEAT; and (c) HyperNEAT.

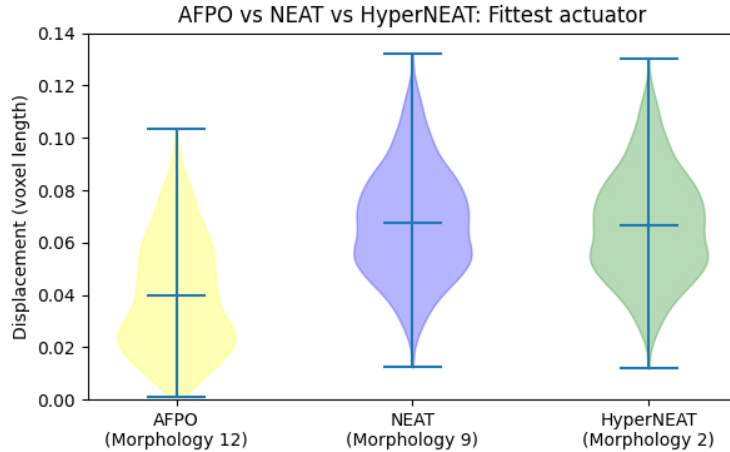


Figure 7: Fittest actuator under: AFPO (left), NEAT (centre), and HyperNEAT (right).

Under NEAT, all morphologies exhibit significant differences, and the data gathered are non-normal (Shapiro-Wilk, Kruskal-Wallis;  $p < 0.01$ ). Based on the previous result, it is feasible to produce a ranking of the performance of the three fittest actuators generated: Morphology 9 > Morphology 16 > Morphology 15 (Dunn's test:  $p < 0.01$ ).

On the other hand, when HyperNEAT is applied, the three fittest morphologies generated show significant differences and non-normality is observed in the data gathered (Shapiro-Wilk, Kruskal-Wallis;  $p < 0.01$ ). Therefore, a ranking focused on performance can be generated: Morphology 2 > Morphology 18 > Morphology 11 (Dunn's test:  $p < 0.01$ ).

Furthermore, Fig. 7 shows violin plots comparing the performance of the fittest actuator morphology produced by AFPO, NEAT and HyperNEAT. Each violin presents the kernel density estimation of the frequency distribution, maximum, minimum and median values of 1000 controller phase offset scenarios. All the morphologies present significant differences, confirmed through the Kruskal-Wallis test ( $p < 0.01$ ). Based on this result, it is possible to rank the performance of the actuators as follows: NEAT > HyperNEAT > AFPO (Dunn's test:  $p < 0.01$ ).

Table 2: Number of passive and contractile voxels of the fittest morphologies produced by AFPO, NEAT, and HyperNEAT.

Approach	Total voxels	Passive voxels	Contractile voxels
AFPO	900	632	268
NEAT	1063	632	431
HyperNEAT	1253	632	621

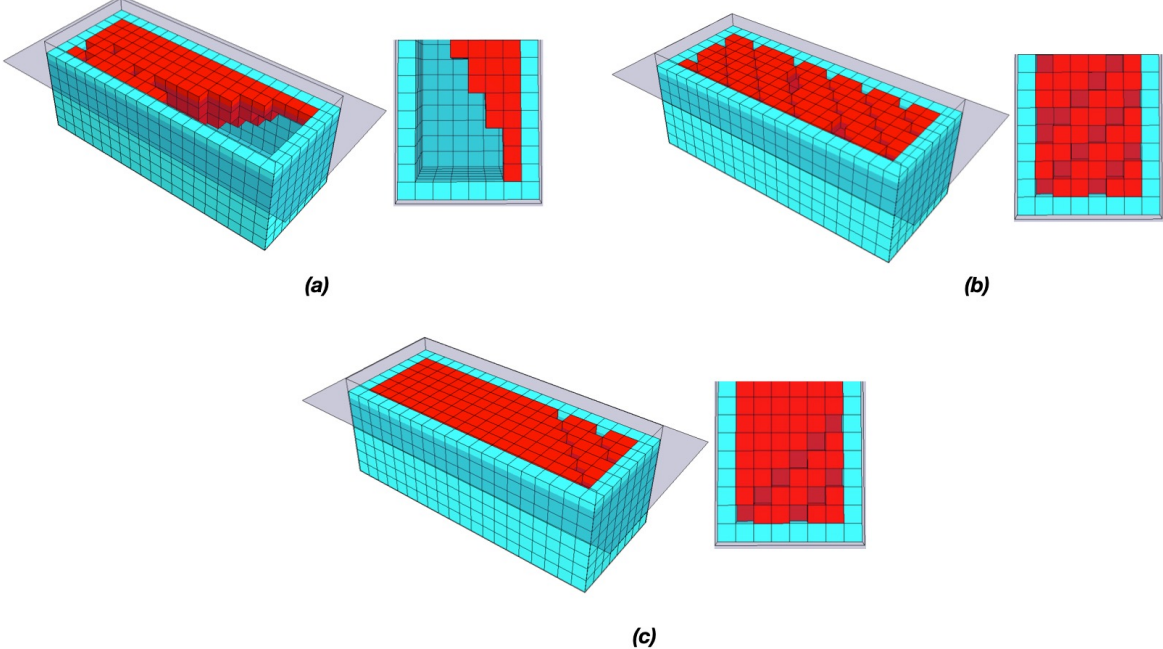


Figure 8: Morphology of the fittest actuator under: (a) AFPO; (b) NEAT; and (c) HyperNEAT. Blue voxels represent passive tissue; red voxels represent contractile tissue.

In general, results suggest that neuroevolution-based approaches, such as NEAT and HyperNEAT, are more adept at producing bendable actuators than those generated by AFPO, regardless of the controller phase offset scenario. This implies that NEAT and HyperNEAT have the potential to create more robust actuators than AFPO. Furthermore, despite the comparable performance of NEAT and HyperNEAT, the former has the edge in producing more robust and, consequently, more bendable actuators.

#### 4.2.3 Identifying the minimum volume of the fittest actuators

Since the morphologies analysed in this research should inform the design of devices in real life whose objective is to manoeuvre within narrow parts of the human body (e.g., blood vessels), the scale of the manufacturing must be significantly minuscule. From this point of view, the fewer voxels the actuator has, the more suitable the catheter employing that actuator. Table 2 presents the number of voxels (passive and contractile) composing the fittest actuators produced by AFPO, NEAT, and HyperNEAT.

Even though AFPO produced the actuator with fewer voxels, its performance is less suitable than the approaches based on NE. In contrast, HyperNEAT produced an actuator whose performance is acceptable; however, the number of voxels, particularly the contractile, is significantly high. Regarding the actuator generated by NEAT, it presents a suitable trade-off between performance and the number of voxels since its performance is the best among the three, and the number of voxels is lower than the number of voxels of the actuator designed by HyperNEAT.

Regarding completeness in the research presented, Fig. 8 depicts the fittest actuator morphologies generated by all approaches. The fittest actuator designed by AFPO (see Fig. 8-a) exhibits a pyramidal pattern consisting of having a few contractile voxels at the bottom and gradually incrementing the number of voxels towards the top of the actuator.

Arguably, the lack of contractile support at the bottom of the actuator affects its bending properties. Furthermore, the fittest actuator generated by NEAT (see Figure 8-b) presents a striped diagonal pattern with no voxels throughout the contractile body composing the actuator. This pattern possibly allows the catheter actuator to bend suitably regardless of the controller phase offset. Finally, the fittest actuator created by HyperNEAT (see Figure 8-c) also exhibits a striped diagonal pattern with no voxels, only in the free end of the actuator. The striped pattern allows the actuator to bend; however, the solid contractile mass on the other end of the actuator arguably attenuates the bending movement.

## 5 Conclusions

This research studied the suitability of NEAT and HyperNEAT as a generator of catheter actuator morphologies. Their capabilities were compared against an implementation of AFPO, a popular multi-objective optimisation approach. The performance analysis was done utilising three metrics: (i) analysing the general performance to find actuators with the maximum displacement possible in the  $yz$  plane; (ii) testing the robustness of those actuators exhibiting the maximum displacement reached (i.e., the fittest actuators); and (iii) determining the fittest actuators with the minimum number of voxels possible. For this analysis, 20 different actuators were generated (i.e., 20 experimental runs were conducted) by each approach.

Results suggest that neuroevolution-based approaches are generally more capable of producing robust catheter actuator morphologies than AFPO due to the genetic operators (i.e., crossover and mutation) induced a broader exploration in the search space, leading to the discovery of fitter individuals than those discovered by AFPO. In addition, the actuator produced by NEAT could outperform the one generated by HyperNEAT. Arguably, the design of the substrate utilised during experimentation affected the performance of HyperNEAT.

Furthermore, the number of voxels plays a crucial role in bending tasks; the fittest actuator found by AFPO exhibited significantly fewer contractile voxels; however, its performance was poor. On the other hand, the fittest actuator generated by NEAT and HyperNEAT showed at least twice the number of voxels of the actuator generated by AFPO. Their performance, nevertheless, overcomes the one from the actuator generated by AFPO. Arguably, the striped no-voxel pattern exhibited by NEAT and HyperNEAT actuators helped to enhance the bending movement.

Considering the results and insights gathered from this research, future work may include the addition of more periodic activation functions, such as cosine and tangent. Following that tactic will help to induce more diverse morphological patterns produced by CPPNs. Another avenue of future work consists of a broader exploration of the number of hidden layers and neurons that may lead to better performance under HyperNEAT. In order to improve the design of the substrate, an approach called *ES-HyperNEAT*, focused on evolving the location of every neuron and the pattern of weights among them, can be implemented [47]. Another crucial aspect of future work will be focused on evolving controllers for the fittest catheters actuators found in this research.

## CRediT authorship contribution statement

**Hugo Alcaraz-Herrera:** Data curation; Formal analysis; Investigation; Methodology; Software; Visualization; Writing - original draft; Writing - review & editing **Michail-Antisthenis Tsompanas:** Conceptualization; Funding acquisition; Methodology; Writing - review & editing **Igor Balaz:** Conceptualization; Funding acquisition; Project administration; Writing - review & editing **Andrew Adamatzky:** Conceptualization; Funding acquisition; Supervision; Writing - review & editing

## Declaration of Competing Interest

The authors declare that they have no known competing financial interests or personal relationships that could have appeared to influence the work reported in this paper.

## Acknowledgement

This project has received funding from the European Union's Horizon Europe research and innovation programme under grant agreement No. 101070328. UWE researchers were funded by the UK Research and Innovation grant No. 10044516.

## References

- [1] *Biomeld reconfigurable organisms*. [https://github.com/Antisthenis/reconfigurable\\_organisms/tree/biomeld\\_dev2](https://github.com/Antisthenis/reconfigurable_organisms/tree/biomeld_dev2). Accessed: 2024-05-19.
- [2] *Reconfigurable organisms*. [https://github.com/skriegman/reconfigurable\\_organisms](https://github.com/skriegman/reconfigurable_organisms). Accessed: 2024-05-19.
- [3] P. AKELLA AND M. CUTKOSKY, *Manipulating with soft fingers: modeling contacts and dynamics*, in Proceedings, 1989 International Conference on Robotics and Automation, IEEE, 1989, pp. 764–769.
- [4] H. ALCARAZ-HERRERA, M.-A. TSOMPANAS, A. ADAMATZKY, AND I. BALAZ, *Neuroevolution algorithms applied in the designing process of biohybrid actuators*. <https://arxiv.org/abs/2408.07671>, 2024.
- [5] S. ARACRI, F. GIORGIO-SERCHI, G. SUARIA, M. E. SAYED, M. P. NEMITZ, S. MAHON, AND A. A. STOKES, *Soft robots for ocean exploration and offshore operations: A perspective*, Soft Robotics, 8 (2021), pp. 625–639.
- [6] J. E. AUERBACH AND J. C. BONGARD, *Evolving cppns to grow three-dimensional physical structures*, in Proceedings of the 12th Annual Conference on Genetic and Evolutionary Computation, GECCO '10, 2010, p. 627–634.
- [7] ———, *Evolving complete robots with cppn-neat: The utility of recurrent connections*, in Proceedings of the 13th Annual Conference on Genetic and Evolutionary Computation, Association for Computing Machinery, 2011.
- [8] P. I. BABUROVA, D. V. KLAJKO, A. LOKTEVA, A. POZHITKOVA, V. RUMYANTCEVA, V. RUMYANTCEVA, I. V. PANKOV, S. TASKAEV, AND V. V. VINOGRADOV, *Magnetic soft robot for minimally invasive urethral catheter biofilm eradication*, ACS nano, 17 (2023), pp. 20925–20938.
- [9] A. BICCHI, *Intrinsic contact sensing for soft fingers*, in Proceedings., IEEE International Conference on Robotics and Automation, IEEE, 1990, pp. 968–973.
- [10] F. Y. CHEN, *Gripping mechanisms for industrial robots: an overview*, Mechanism and Machine Theory, 17 (1982), pp. 299–311.
- [11] N. CHENEY, J. BONGARD, AND H. LIPSON, *Evolving soft robots in tight spaces*, in Proceedings of the 2015 Annual Conference on Genetic and Evolutionary Computation, GECCO '15, 2015, p. 935–942.
- [12] J. CLUNE, B. E. BECKMANN, C. OFRIA, AND R. T. PENNOCK, *Evolving coordinated quadruped gaits with the hyperneat generative encoding*, in 2009 IEEE Congress on Evolutionary Computation, 2009, pp. 2764–2771.
- [13] J. CLUNE, C. OFRIA, AND R. T. PENNOCK, *The sensitivity of hyperneat to different geometric representations of a problem*, in Proceedings of the 11th Annual Conference on Genetic and Evolutionary Computation, 2009, p. 675–682.
- [14] D. B. D'AMBROSIO AND K. O. STANLEY, *Generative encoding for multiagent learning*, in Proceedings of the 10th Annual Conference on Genetic and Evolutionary Computation, 2008, p. 819–826.
- [15] M. FRIEDMAN AND K. KRAUTHAUSEN, *Interview with barbara mazzolai: Plants, plantoids, and active materials*, Active Materials, (2021), p. 129.
- [16] C. GILLESPIE AND C. GILLESPIE, *Optical control of electrostatic actuators using amorphous silicon*, strain, 1 (1985), p. 300.
- [17] D. E. GOLDBERG AND J. RICHARDSON, *Genetic algorithms with sharing for multimodal function optimization*, in Proceedings of the Second International Conference on Genetic Algorithms on Genetic Algorithms and Their Application, 1987, p. 41–49.
- [18] T. GOPESH, J. H. WEN, D. SANTIAGO-DIEPPA, B. YAN, J. S. PANNELL, A. KHALESSI, A. NORBASH, AND J. FRIEND, *Soft robotic steerable microcatheter for the endovascular treatment of cerebral disorders*, Science robotics, 6 (2021), p. eabf0601.
- [19] J. HILLER AND H. LIPSON, *Dynamic simulation of soft multimaterial 3d-printed objects*, Soft robotics, 1 (2014), pp. 88–101.
- [20] S. HIROSE AND Y. UMETANI, *The development of soft gripper for the versatile robot hand*, Mechanism and machine theory, 13 (1978), pp. 351–359.
- [21] G. S. HORNBYS, *Alps: the age-layered population structure for reducing the problem of premature convergence*, in Proceedings of the 8th Annual Conference on Genetic and Evolutionary Computation, 2006, p. 815–822.
- [22] J.-H. HSIAO, J.-Y. CHANG, AND C.-M. CHENG, *Soft medical robotics: clinical and biomedical applications, challenges, and future directions*, Advanced Robotics, 33 (2019), pp. 1099–1111.

[23] X. HU, Y. ZHOU, M. LI, J. WU, G. HE, AND N. JIAO, *Catheter-assisted bioinspired adhesive magnetic soft millirobot for drug delivery*, *Small*, 20 (2024), p. 2306510.

[24] S. K. JHA AND F. JOSHESKI, *Artificial evolution using neuroevolution of augmenting topologies (neat) for kinetics study in diverse viscous mediums*, *Neural Computing and Applications*, 29 (2018).

[25] G. L. KENALEY AND M. R. CUTKOSKY, *Electrorheological fluid-based robotic fingers with tactile sensing*., in *ICRA*, 1989, pp. 132–136.

[26] T. KIMURA, R. NIYAMA, AND Y. KUNIYOSHI, *Modularized genotype combination to design multiobjective soft-bodied robots*, in *2021 IEEE 4th International Conference on Soft Robotics (RoboSoft)*, 2021, pp. 295–301.

[27] G. KLAMBAUER, T. UNTERTHINER, A. MAYR, AND S. HOCHREITER, *Self-normalizing neural networks*, in *Proceedings of the 31st International Conference on Neural Information Processing Systems*, 2017, p. 972–981.

[28] S. KRIEGMAN, D. BLACKISTON, M. LEVIN, AND J. BONGARD, *A scalable pipeline for designing reconfigurable organisms*, *Proceedings of the National Academy of Sciences*, 117 (2020), pp. 1853–1859.

[29] Y. S. KWON, J. HOU, E. A. JONCKHEERE, AND S. HAYATI, *A robot with improved absolute positioning accuracy for ct guided stereotactic brain surgery*, *IEEE transactions on biomedical engineering*, 35 (1988), pp. 153–160.

[30] V. LEVERING, Q. WANG, P. SHIVAPOOJA, X. ZHAO, AND G. P. LÓPEZ, *Soft robotic concepts in catheter design: an on-demand fouling-release urinary catheter*, *Advanced healthcare materials*, 3 (2014), pp. 1588–1596.

[31] Y. LI, J. PEINE, M. MENCATELLI, J. WANG, J. HA, AND P. E. DUPONT, *A soft robotic balloon endoscope for airway procedures*, *Soft Robotics*, 9 (2022), pp. 1014–1029.

[32] H. LIPSON, *Challenges and opportunities for design, simulation, and fabrication of soft robots*, *Soft Robotics*, 1 (2014), pp. 21–27.

[33] C. MAJIDI, *Soft robotics: a perspective—current trends and prospects for the future*, *Soft robotics*, 1 (2014), pp. 5–11.

[34] B. MAZZOLAI, C. LASCHI, P. DARIO, S. MUGNAI, AND S. MANCUSO, *The plant as a biomechatronic system*, *Plant signaling & behavior*, 5 (2010), pp. 90–93.

[35] B. MAZZOLAI, V. MATTOLI, L. BECCAI, AND E. SINIBALDI, *Emerging technologies inspired by plants*, *Bioinspired approaches for human-centric technologies*, (2014), pp. 111–132.

[36] B. MAZZOLAI, G. MELONI, AND A. DEGL'INNOCENTI, *Can a robot grow? plants give us the answer*, in *Bioinspiration, Biomimetics, and Bioreplication 2017*, vol. 10162, SPIE, 2017, pp. 24–33.

[37] B. MAZZOLAI AND P. SALVINI, *On robots and plants: The case of the plantoid, a robotic artifact inspired by plants*, in *Plant Ethics*, Routledge, 2018, pp. 221–230.

[38] G. METHENITIS, D. HENNES, D. IZZO, AND A. VISSER, *Novelty search for soft robotic space exploration*, in *Proceedings of the 2015 annual conference on Genetic and Evolutionary Computation*, 2015, pp. 193–200.

[39] E. MILANA, *Soft robotics for infrastructure protection*, *Frontiers in Robotics and AI*, 9 (2022), p. 1026891.

[40] S. MINTCHEV, D. ZAPPETTI, J. WILLEMIN, AND D. FLOREANO, *A soft robot for random exploration of terrestrial environments*, in *2018 IEEE International Conference on Robotics and Automation (ICRA)*, IEEE, 2018, pp. 7492–7497.

[41] R. R. MURPHY, *Marsupial and shape-shifting robots for urban search and rescue*, *IEEE Intelligent Systems and their applications*, 15 (2000), pp. 14–19.

[42] N. NEGROPONTE, *Soft architecture machines*, The MIT Press, 1976.

[43] C. S. X. NG AND G. Z. LUM, *Untethered soft robots for future planetary explorations?*, *Advanced Intelligent Systems*, 5 (2023), p. 2100106.

[44] C. C. NGUYEN, T. TEH, M. T. THAI, P. T. PHAN, T. T. HOANG, H. LOW, J. DAVIES, E. NICOTRA, N. H. LOVELL, AND T. N. DO, *Bidirectional soft robotic catheter for arrhythmia treatment*, in *2022 International Conference on Robotics and Automation (ICRA)*, IEEE, 2022, pp. 9579–9585.

[45] C. C. NGUYEN, M. T. THAI, T. T. HOANG, J. DAVIES, P. T. PHAN, K. ZHU, L. WU, M. A. BRODIE, D. TSAI, Q. P. HA, ET AL., *Development of a soft robotic catheter for vascular intervention surgery*, *Sensors and Actuators A: Physical*, 357 (2023), p. 114380.

[46] T. PATINO, R. MESTRE, AND S. SANCHEZ, *Miniaturized soft bio-hybrid robotics: a step forward into healthcare applications*, *Lab on a Chip*, 16 (2016), pp. 3626–3630.

[47] S. RISI AND K. O. STANLEY, *An Enhanced Hypercube-Based Encoding for Evolving the Placement, Density, and Connectivity of Neurons*, *Artificial Life*, 18 (2012), pp. 331–363.

[48] ——, *Confronting the challenge of learning a flexible neural controller for a diversity of morphologies*, in Proceedings of the 15th Annual Conference on Genetic and Evolutionary Computation, GECCO '13, 2013, p. 255–262.

[49] J. ROGATINSKY, D. RECCO, J. FEICHTMEIER, Y. KANG, N. KNEIER, P. HAMMER, E. O'LEARY, D. MAH, D. HOGANSON, N. V. VASILYEV, ET AL., *A multifunctional soft robot for cardiac interventions*, *Science Advances*, 9 (2023), p. eadi5559.

[50] D. RUS AND M. T. TOLLEY, *Design, fabrication and control of soft robots*, *Nature*, 521 (2015), pp. 467–475.

[51] A. SADEGHI, A. MONDINI, E. DEL DOTTORE, V. MATTOLI, L. BECCAI, S. TACCOLA, C. LUCAROTTI, M. TOTARO, AND B. MAZZOLAI, *A plant-inspired robot with soft differential bending capabilities*, *Bioinspiration & biomimetics*, 12 (2016), p. 015001.

[52] M. D. SCHMIDT AND H. LIPSON, *Age-fitness pareto optimization*, in Proceedings of the 12th Annual Conference on Genetic and Evolutionary Computation, 2010, p. 543–544.

[53] A. SCHULZ, C. SUNG, A. SPIELBERG, W. ZHAO, R. CHENG, E. GRINSPUN, D. RUS, AND W. MATUSIK, *Interactive robogami: An end-to-end system for design of robots with ground locomotion*, *The International Journal of Robotics Research*, 36 (2016), pp. 1131–1147.

[54] K. STANLEY AND R. MIIKKULAINEN, *Efficient evolution of neural network topologies*, in Proceedings of the 2002 Congress on Evolutionary Computation. CEC'02 (Cat. No.02TH8600), vol. 2, 2002, pp. 1757–1762 vol.2.

[55] K. O. STANLEY, *Compositional pattern producing networks: A novel abstraction of development*, *Genetic Programming and Evolvable Machines*, 8 (2007), pp. 131–162.

[56] K. O. STANLEY, D. B. D'AMBROSIO, AND J. GAUCI, *A Hypercube-Based Encoding for Evolving Large-Scale Neural Networks*, *Artificial Life*, 15 (2009), pp. 185–212.

[57] K. O. STANLEY AND R. MIIKKULAINEN, *Evolving neural networks through augmenting topologies*, *Evolutionary Computation*, 10 (2002), pp. 99–127.

[58] F. TANAKA AND C. ARANHA, *Co-evolving morphology and control of soft robots using a single genome*, in 2022 IEEE Symposium Series on Computational Intelligence (SSCI), 2022, pp. 1235–1242.

[59] M.-A. TSOMPANAS, *Incremental growth on compositional pattern producing networks based optimization of biohybrid actuators*, in International Conference on the Applications of Evolutionary Computation (Part of EvoStar), S. Smith, J. Correia, and C. Cintrano, eds., Cham, 2024, Springer Nature Switzerland, pp. 275–289.

[60] M.-A. TSOMPANAS AND I. BALAZ, *Outline of an evolutionary morphology generator towards the modular design of a biohybrid catheter*, *Frontiers in Robotics and AI*, 11 (2024).

[61] E. C. R. G. (UCF), *The hypercube-based neuroevolution of augmenting topologies (hyperneat) users page*. <http://eplex.cs.ucf.edu/hyperNEATpage/>, 2016. Accessed: March 24th, 2024.

[62] X. WANG, Q. ZHANG, D. SHEN, AND J. CHEN, *A novel rescue robot: Hybrid soft and rigid structures for narrow space searching*, in 2019 IEEE International Conference on Robotics and Biomimetics (ROBIO), IEEE, 2019, pp. 2207–2213.

[63] R. WEN, Z. GUO, T. ZHAO, X. MA, Q. WANG, AND Z. WU, *Neuroevolution of augmenting topologies based muscular-skeletal arm neurocontroller*, in 2017 IEEE International Instrumentation and Measurement Technology Conference (I2MTC), 2017, pp. 1–6.

[64] T. WEN, J. HU, J. ZHANG, X. LI, S. KANG, AND N. ZHANG, *Design, performance analysis, and experiments of a soft robot for rescue*, *Journal of Mechanisms and Robotics*, 16 (2024).

[65] Y. YANG, J. WANG, L. WANG, Q. WU, L. LING, Y. YANG, S. NING, Y. XIE, Q. CAO, L. LI, ET AL., *Magnetic soft robotic bladder for assisted urination*, *Science Advances*, 8 (2022), p. eabq1456.

[66] J. YOSINSKI, J. CLUNE, D. HIDALGO, S. NGUYEN, J. C. ZAGAL, AND H. LIPSON, *Evolving robot gaits in hardware: the HyperNEAT generative encoding vs. parameter optimization*, in Proceedings of the 2023 Artificial Life Conference, 2021, p. 134.

[67] C. ZHOU, Y. YANG, J. WANG, Q. WU, Z. GU, Y. ZHOU, X. LIU, Y. YANG, H. TANG, Q. LING, ET AL., *Ferromagnetic soft catheter robots for minimally invasive bioprinting*, *Nature communications*, 12 (2021), p. 5072.